Hindawi
Shock and Vibration
Volume 2017, Article ID 5624534, 11 pages
https://doi.org/10.1155/2017/5624534

Research Article

Effect of Nonsmooth Nose Surface of the Projectile on Penetration Using DEM Simulation

Jing Han,[1] Dong Li,[1] Wenhao Wang,[1] and Zhigang Chen[1,2]

[1]*College of Mechatronic Engineering, North University of China, Shanxi, Taiyuan 030051, China*
[2]*National Defense Key Discipline Laboratory of Underground Target Damage, Shanxi, Taiyuan 030051, China*

Correspondence should be addressed to Jing Han; 1368284410@qq.com

Received 17 July 2017; Revised 19 September 2017; Accepted 28 September 2017; Published 21 November 2017

Academic Editor: Giosuè Boscato

Copyright © 2017 Jing Han et al. This is an open access article distributed under the Creative Commons Attribution License, which permits unrestricted use, distribution, and reproduction in any medium, provided the original work is properly cited.

The nonsmooth body surface of the reptile in nature plays an important role in reduction of resistance and friction when it lives in a soil environment. To consider whether it was feasible for improving the performance of penetrating projectile we investigated the influence of the convex as one of nonsmooth surfaces for the nose of projectile. A numerical simulation study of the projectile against the concrete target was developed based on the discrete element method (DEM). The results show that the convex nose surface of the projectile is beneficial for reducing the penetration resistance greatly, which is also validated by the experiments. Compared to the traditional smooth nose structure, the main reason of difference is due to the local contact normal pressure, which increases dramatically due to the abrupt change of curvature caused by the convex at the same condition. Accordingly, the broken particles of the concrete target obtain more kinetic energy and their average radial flow velocities will drastically increase simultaneously, which is in favor of decreasing the interface friction and the compaction density of concrete target around the nose of projectile.

1. Instruction

The penetrating problem of the projectile against geological target has already been the focus of research for a long time. It has been found that there are many factors that influence the penetration performance. The nose of the projectile, named shape function in cavity-expansion theory, could determine the impact pressure [1] and the interface friction [2] between projectile and target. Therefore, as one of the most important factors, it can affect the penetrating resistance directly.

In the process of natural evolution, the reptile, such as lizard, dung beetle, and pangolin, has its special body surface morphology, which is classified into five types: groove, rib, scale, convex, and concave according to different shapes. The bionic research has discovered that these specific structures can play important roles in reducing soil resistance and friction when the reptile lives in the geological environment [3]. At present, the explanation for this above phenomenon is attributed to the following aspects [4–6].

(i) When the reptile moves in the soil, the nonsmooth surface can decrease the real contact area, resulting in the reduction of friction accordingly.

(ii) The nonsmooth surface of the reptile is able to change the movement pattern of the contact soil particle from sliding to rolling. Therefore, it decreases the friction force and has ability of antiwear correspondingly.

(iii) The soil compacted density around the reptile could decrease because the groove and concave nonsmooth surface can hold a certain amount of the soil fragments.

Inspired by the nonsmooth surface structure, the question is can it be applied to design the projectile nose to deduce the penetration resistance and abrasion? We think it is essential to research the difference of penetration caused by the convex surface.

Since the discrete element method (DEM) was developed by Cundall and Strack in 1979 [7], the constitutive relations

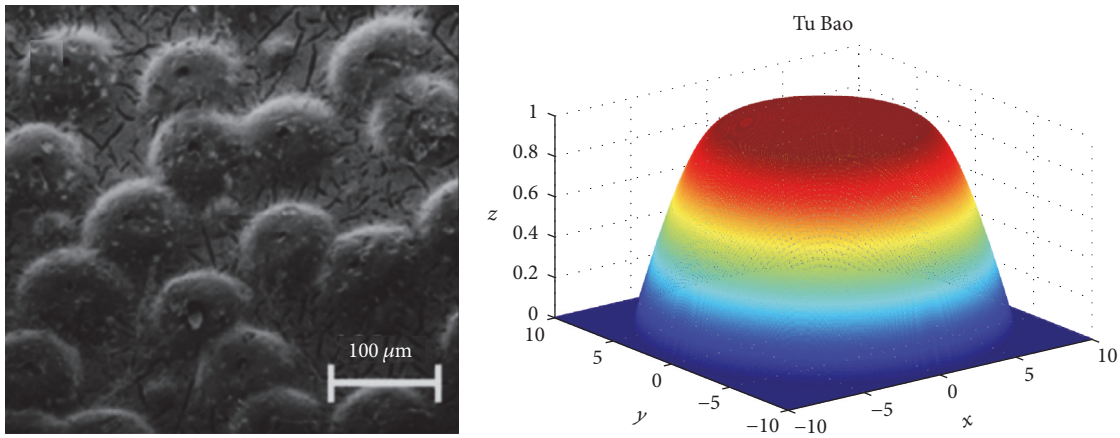

Figure 1: The convex nonsmooth surface of the dung beetle.

of the rock and concrete can be reasonably described by the bonded particle model [8]. Recently, it was proven that this approach is a powerful tool in understanding the projectile penetration and the soil or concrete target fracture [9–11]. More importantly, it can preferably reflect the characteristics of interface friction [12], wear [13], energy transmission, and the movement of broken materials [14]. These advantages will be beneficial to understand the effect of nonsmooth surface on the projectile nose contact with the crashed particle of the geological target.

2. The Structure Selection of Nonsmooth Surface for Projectile Nose

The dung beetle, as the typical soil reptile, has three kinds of nonsmooth structure (convex, concave, and groove) simultaneously, which are distributed in its different parts of body. In particular, it has been found that the convex structure, mostly distributing in the labrum and claw of the dung beetle, squeezes and rubs against the soil frequently. The shape of the convex on beetle surface is just like an upturned saucer and its bottom surface transits smoothly (the microscopic image and model of convex, see Figures 1(a) and 1(b), respectively). The math relationship can be described as

$$z = h \sin\left(\frac{R_1 + R_2}{2R_2}\pi - \frac{\sqrt{x^2 + y^2}}{2R_2}\pi\right). \quad (1)$$

Similarly, considering the severity of impact and friction of projectile nose, the convex was selected as the nonsmooth unit in this paper. Meanwhile, in order to facilitate easily in the future, the shape of convex was simplified as a spherical cap and began to layout from a certain distance with the nose tip of the projectile. The experiment discovered that the average convex diameter of the dung beetle antenna is 5~10 μm, which is 1/50~1/100 times the antenna approximately [15]. Therefore, in this paper, comparing with the 22.5 mm radius of the projectile the convex diameter was preliminary set to 0.9 mm. The convex surface of the projectile was designed as shown in Figure 2.

3. DEM Modeling

3.1. PBM Model. The DEM modeling of the geological materials is based on bonding or gluing a packed distribution of sphere particles together for simulating its breakage and its propagation. The interaction between any two interacting sphere particles can be represented by the normal and shear force as well as their moments (as illustrated by schematic graph in Figure 3(a)), which are described, respectively, by a force-displacement and Newton-Euler equations. In this paper, the equivalent model so-called Hertz-Mindlin with Bonding as one of the particle bonded model (PBM) was used to simulate the concrete properties at the microscopic level. The expression is written as

$$\begin{aligned} F_n &= F_n^{t-1} + k_n A \Delta U_n \\ F_s &= F_s^{t-1} + k_s A \Delta U_t \\ T_n &= T_n^{t-1} + k_s J \Delta \Theta_n \\ T_s &= T_s^{t-1} + k_n \frac{J}{2} \Delta \Theta_s, \end{aligned} \quad (2)$$

where $A = \pi R_B^2$, $J = (1/2)\pi R_B^4$, R_B is the bond radius of contact particle, and ΔU_n and ΔU_s are relative displacements in the normal and tangential direction. $\Delta\Theta_n$ and $\Delta\Theta_s$ are relative angular displacements in the normal and shear direction.

Accordingly, the overall behaviors of the packed particle are determined by the loading modes, bond stiffness, and stress criteria as shown in Figure 3(b). Once the interface strength is exceeded by the cohesive force in either shear or normal direction, the cohesive bond will be broken.

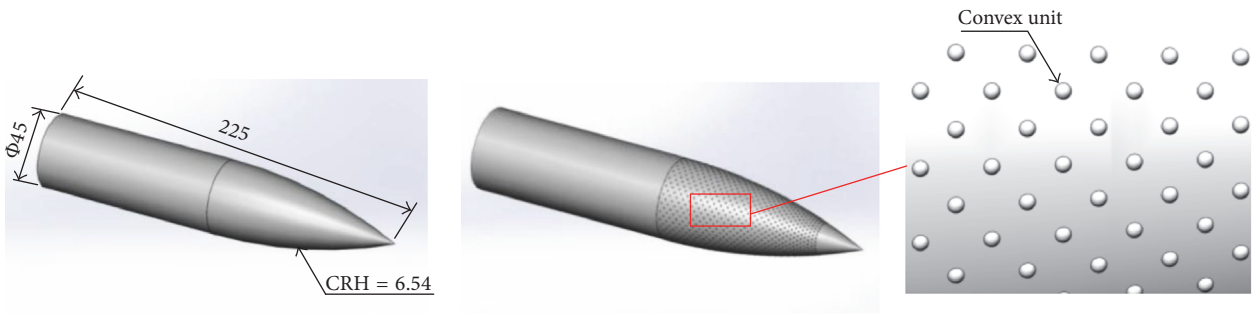

Figure 2: The projectile with convex nonsmooth nose surface.

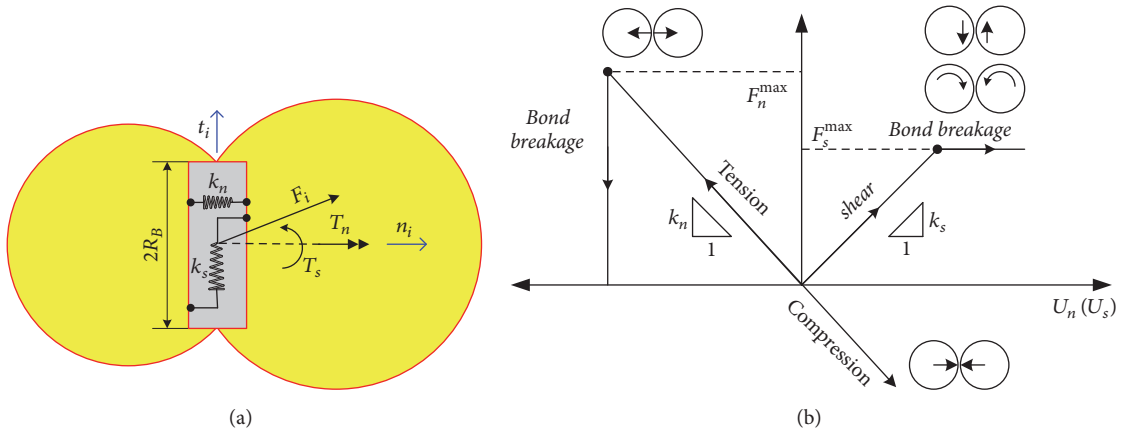

Figure 3: Schematic of forces and moments induced in the BPM model: (a) model of the bonded particles and (b) different breaking models for the adhere bond.

Specifically, the failure criterion is predetermined using the following equations.

$$F_n^{\max} < \frac{\sigma_c}{A} - 2\frac{T_n}{JA}R_B$$
$$F_s^{\max} < \frac{\tau_c}{A} - 2\frac{T_s}{JA}R_B. \quad (3)$$

3.2. DEM Parameters. In order to better conform to the reality of material there is a need to demarcate the parameter of DEM. First, the particle shape and size of the DEM concrete target need to be chosen so that a sufficient quality of breakage is achieved in the process of penetration. In most cases, the particle of concrete or rock DEM materials is unified set sphere with Gaussian distribution. It is noted that particles of the DEM model do not represent individual grains but rather a proportion of the subject material at mesoscopic level. Therefore, the diameter of particle is greater than the grains used in real concrete structure. Moreover, from the materials composition the equivalent diameter of the coarse aggregate normally exceeds 4.75 mm and the mass proportion of them reaches 70% approximately. Thus in this work all particles had a diameter distribution size between 0.005 m and 0.02 m and the total number of discrete elements generated in the reference case specimen was about 34000.

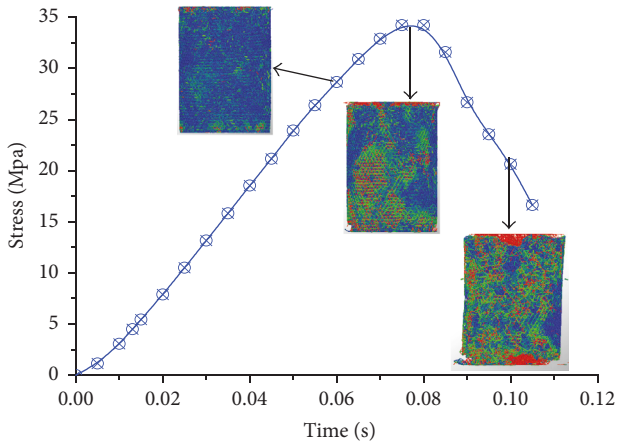

Figure 4: The stress history of the quasi-static test for the concrete DEM model.

Second, the value of these PBM parameters should be validated by the simulation of quasi-static triaxial compression or the Brazilian splitting test, which is similar to previous work [12]. As can be seen in Figure 4, the mechanical properties of DEM model for this simulation were as close as possible to the concrete with a 30 Gpa Young's modulus

Table 1: Particle bonding parameters for concrete.

Parameters	Value
Density ρ_c (kg/m^3)	2500
Poisson's ratio λ_c	0.35
Shear modulus G_c (Pa)	$1.2E + 10$
Normal stiffness k_n (N/m^3)	$7E + 10$
Shear stiffness k_s (N/m^3)	$1.4E + 10$
Normal critical stress σ_c (Pa)	$2.3E + 07$
Shear critical stress τ_c (Pa)	$2.3E + 06$
Bonded disc radius R_B (m)	0.0025
Coefficient of static friction f_s	0.3
Coefficient of restitution e	0.5
Coefficient of rolling friction f_r	0.001

and a 35 MPa compressive strength after adjusting the PBM parameters. In addition, it has been proved that the material inertial plays the major role in compression mode [13], so the strain-rate effect of DEM simulation does not need to be considered separately. Here, the input numerical data are listed in Table 1.

4. Simulation Results and Discussion

In this simulation, the cylindrical shape target with 0.25 m diameter and 0.6 m height was imparted normally by a convex nose surface projectile. As mentioned in Section 2, the diameter of spherical cap for convex unit was selected as Φ0.9 mm with variation of height h_{convex} = 0.1 mm, 0.2 mm, and 0.3 mm, which was also compared with traditional smooth surface one represented by the term of h_{convex} = 0 mm. For every type of nonsmooth surface, the linear density of the convex distribution is not less than 0.266. In view of theoretical formulations of DEM both the projectile and the particles are assumed rigid, while the rigid bodies are allowed to overlap with one another using PBM contact approach.

4.1. Influence of Convex on the Interfacial Behaviors

4.1.1. Force History of the Projectile. As a whole, the projectile against the target with the constant velocity, the total penetrating process includes two stages. At the beginning of the penetration, the average resistance force on the nose of projectile increases linearly with the penetration distance due to the developing of the contact zone between projectile and target. Once the nose of projectile is completely into the target the penetration reaches a steady state that results in approaching constant value of the penetration resistance [16]. In other words the state of penetration for the projectile at some speed can be represented by the limiting penetration resistance correspondingly.

Figure 5 shows comparison of convex nonsmooth nose surface to conventional smooth surface projectile for penetration resistance as a function of penetration distance at the constant penetration velocity v = 450 m/s. As can be seen, the penetration forces for two-type projectile vary with

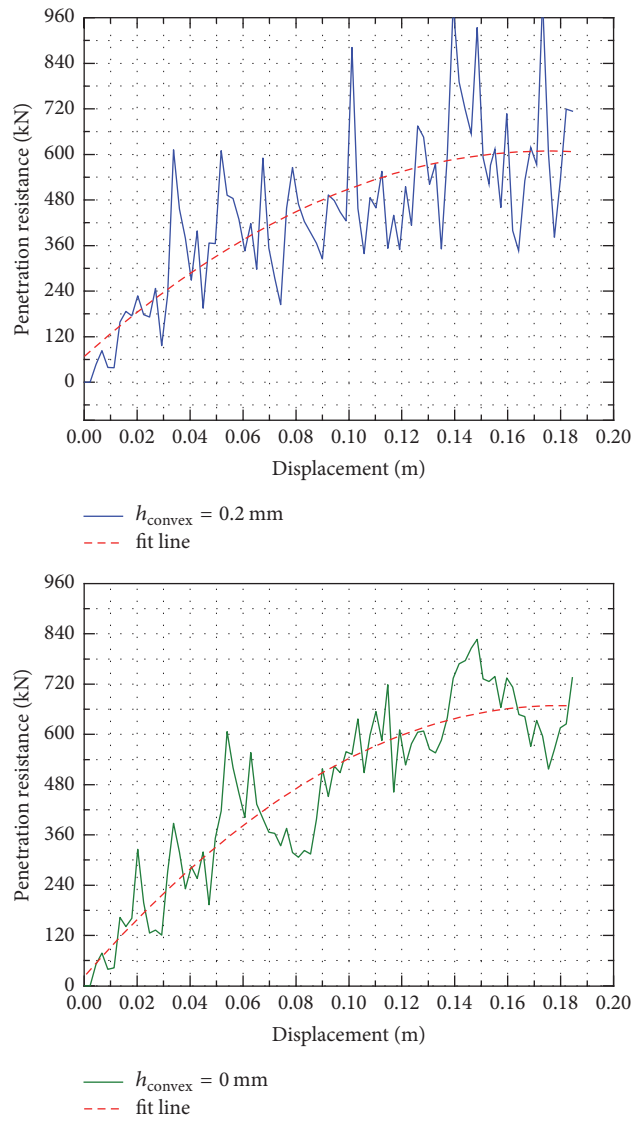

Figure 5: Penetration resistance of different surface nose as a function of the penetration depth. The constant penetration velocity is 450 m/s.

displacement nonlinearly. In the penetrating process, the fluctuation of the resistance is mainly due to the discontinuity contact between projectile nose surface and packed particles. However, in contrast with the traditional projectile, the fluctuation ranges of penetration resistance for convex surface h_{convex} = 0.2 mm expanded significantly. From their fit lines, there are similar trends that the average penetration resistance is approximately proportional to distance until the projectile nose depth reaches 0.15 m. On the other side the average limiting penetration resistance (obtained from the fitting curve) is only near 6.0×10^5 N for convex surface and more than 6.6×10^5 N for smooth surface, respectively, which is decreased obviously.

Figure 6(a) shows the total pressure history of different projectile nose structure with the constant velocity of 450 m/s. It can be clearly seen that the convex nose surface

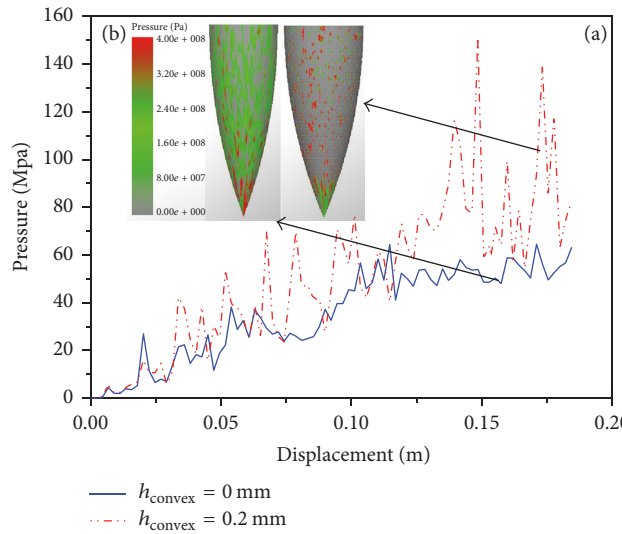

FIGURE 6: Influence of convex on the contact pressure between projectile and concrete target. The pressure cloud maps were snapped at 0.3 ms while the distance is 0.14 m: (a) contact pressure curves and (b) cloud map of contact pressure distribution.

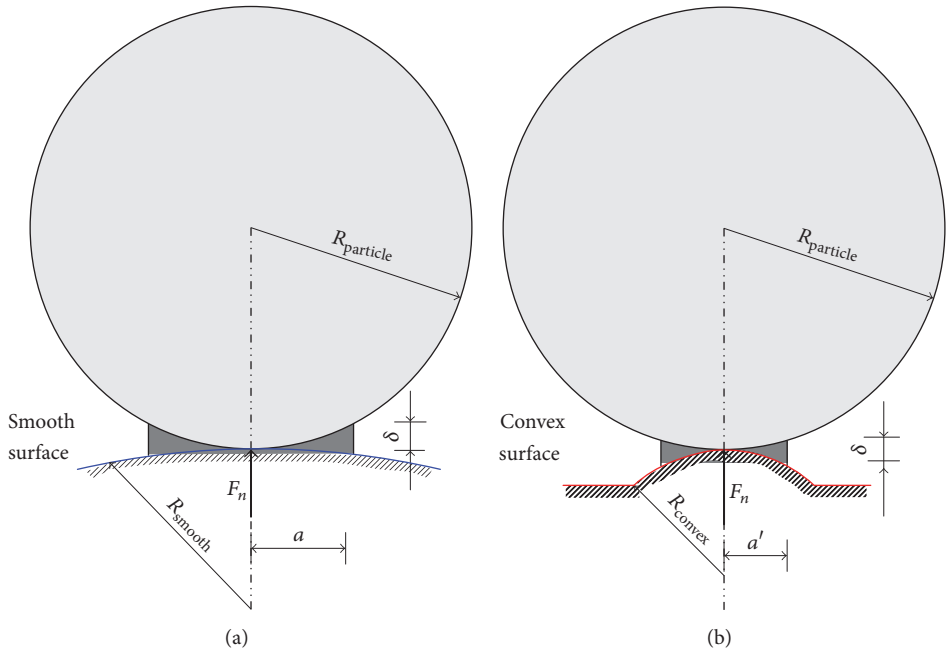

FIGURE 7: Contact model of different surface: (a) smooth surface contacts with particle and (b) convex surface contacts with particle.

caused a higher total contact pressure than the smooth one in the penetrating process. As can be seen in Figure 7 this effect is mainly due to the increase of local surface curvature giving rise by the convex unit which is changed from $1/R_{smooth}$ to $1/R_{convex}$. According to (4) found by Hertz theory, higher curvature gives smaller contact radius a and finally causes higher contact stress that is calculated by F_n/a.

$$a = \sqrt{\frac{3F_n\left[\left(1-\nu_c{}^2\right)/E_c + \left(1-\nu_s{}^2\right)/E_s\right]}{4\left(1/R_{particle} + 1/R_{surface}\right)}}, \quad (4)$$

where a is contact radius, F_n is contact force between particle and projectile surface, and ν_c, ν_s, and E_c, E_s are Poisson's ratio and elasticity modulus of concrete particles and projectile, respectively.

In addition, when adopting convex nose surface on projectile, the pattern of contact pressure for it has changed from cloud flake to mottling, as shown in Figure 6(b). Their nose tip zone of convex before height of 0.25 mm is subjected to less contact pressure and the total area of nonsmooth nose surface between projectile and target also decreases significantly. This result also indicates that less contact area

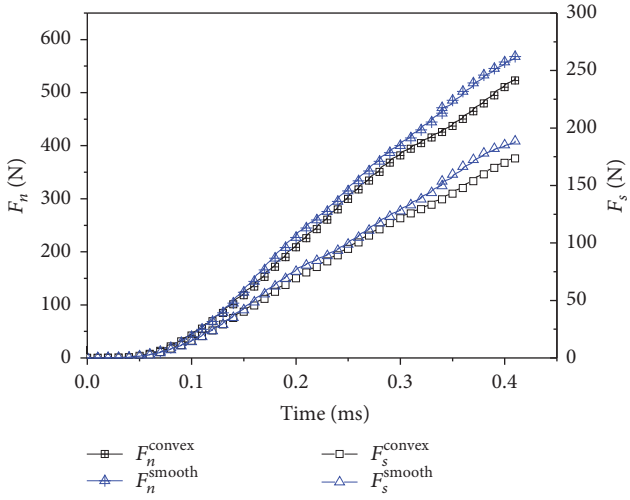

Figure 8: Average bond force of the target particle.

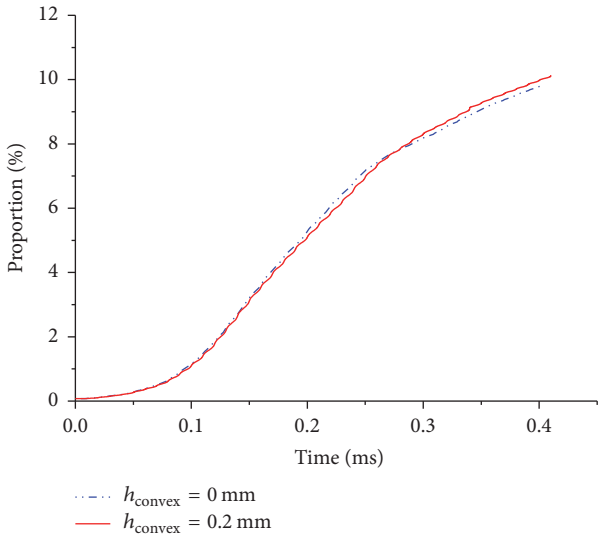

Figure 9: Proportion of broken bonds.

of the convex surface is beneficial to resist the effect of wear and mass erosion in the process of penetration.

4.1.2. Force History of PBM Bonds. Figure 8 shows the bond force history of particle target at constant velocity of 450 m/s. We can also see that both average normal forces F_n and shear one F_s among bonded particles increased simultaneously 0.3 ms later. In other words, it can be concluded that the additional contact force contributes to speed up the breakage of adhered particle around the projectile. Such result leads to increasing the accumulated proportion of broken bond, after the projectile nose contacted with target completely (the penetration distance is more than the projectile nose length by 0.113 m, with the corresponding time being 0.3 ms), as shown in Figure 9. Meanwhile, the increasing of contact forces also can be reflected from Figure 6(b), which reached 400 Mpa especially near the convex hull.

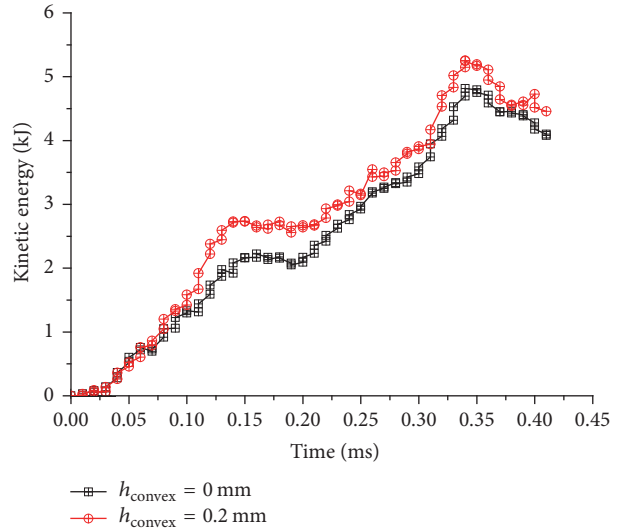

Figure 10: The effect of the convex surface on the total kinetic energy history.

4.1.3. Kinetic Energy Distribution of the Broken Particle. During the penetration, the broken particle of the target, damaged by the convex surface nosed projectile, obtained more than the total kinetic energy after 0.1 ms (see in Figure 10). From Figures 11(a) and 11(b) it is further illustrated that because of the convex unit more kinetic energy is transferred to the particles located in the radial direction of the nose tip. The reason is that the direction of velocity for broken particles may be changed and more particles obtain greater flow speed sequentially in radial direction when the convex hull comes in contact with the concrete target (see in Figure 12). Thus, the compaction density of concrete target around the tip of projectile decreases accordingly, which also improves the effect of antidrag and antiwear simultaneously.

4.2. Prediction of Normal Penetrating. The simulation results using the above DEM method were only on behalf of the penetration state at a certain velocity. In order to directly predict penetration performance of the convex surface projectile, the average limiting penetration resistance under different velocities should be firstly calculated by DEM simulations and fitted a function related to the velocity. Finally, the prediction of penetration depth using the following formula (5) can be calculated by this fit function.

$$
\begin{aligned}
V_{i+1} &= \left(V_i^2 + 2a_i\Delta z\right)^{1/2} \\
\Delta t &= \frac{\left(V_{i+1} - V_i\right)}{a_i} \\
a_{i+1} &= \frac{f\left(z_{i+1}, V_{i+1}\right)}{m} \\
z_{i+1} &= z_i + \Delta z \\
t_{i+1} &= t_i + \Delta t,
\end{aligned}
\tag{5}
$$

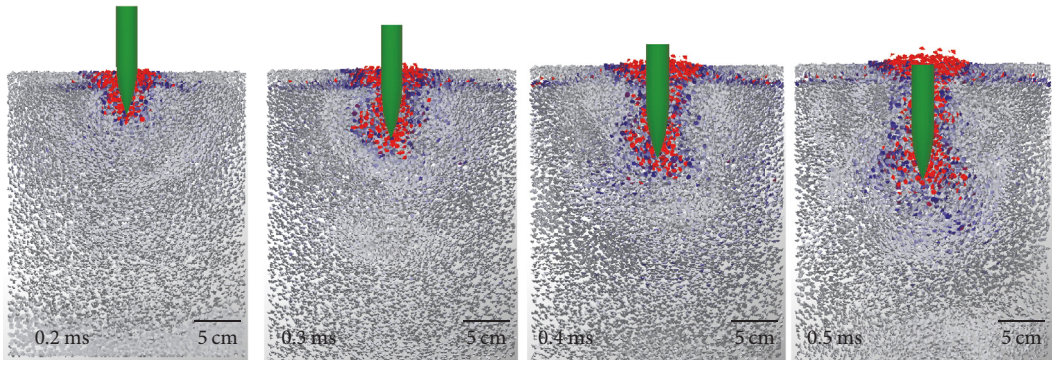

(a) Smooth surface

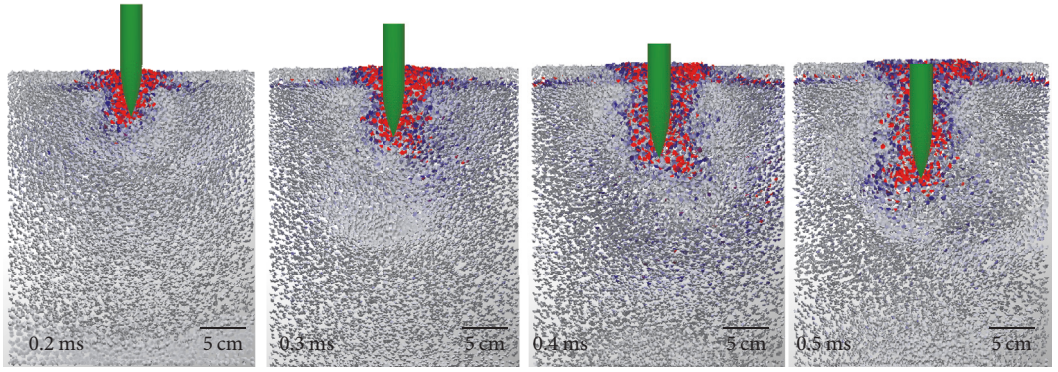

(b) Convex surface

Figure 11: Kinetic energy distribution for the target particle: (a) smooth surface and (b) convex surface.

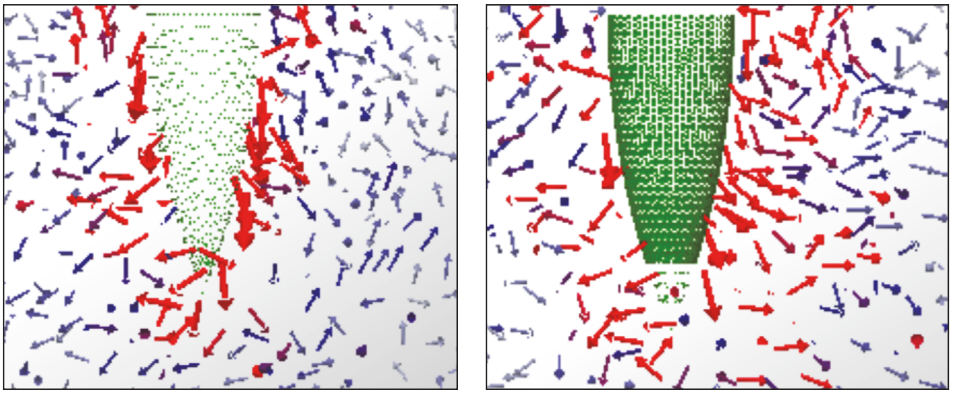

(a) Smooth surface (b) Convex surface

Figure 12: Comparison of the velocity of broken particles around the projectile nose at 0.4 ms: (a) smooth surface and (b) convex surface.

where V_i and a_i are the velocity and acceleration at time t_i, respectively. z_i is the penetration depth. $f(z_i, V_i)$ is the function of penetration resistance. m is the mass of the projectile. Δt and Δz are the increment of time and penetration depth.

Figure 13 shows the results of penetration acceleration calculated by DEM simulation and Forrestal empirical formula, respectively [17, 18]. In this case, the mass of projectile and initial velocity were set to 1.44 kg and 450 m/s, respectively. It is observed that the DEM simulation results have good accuracy and coincide with the theory analysis. The variation trend of acceleration obtained by DEM simulation decreased more rapidly. We think the reason is that the penetration resistance of Forrestal empirical formula mainly comes from hydrostatic pressure provided by the compressive strength of the concrete target, which neglects the friction effect. In DEM contact model, however, it attributes to the bond strength,

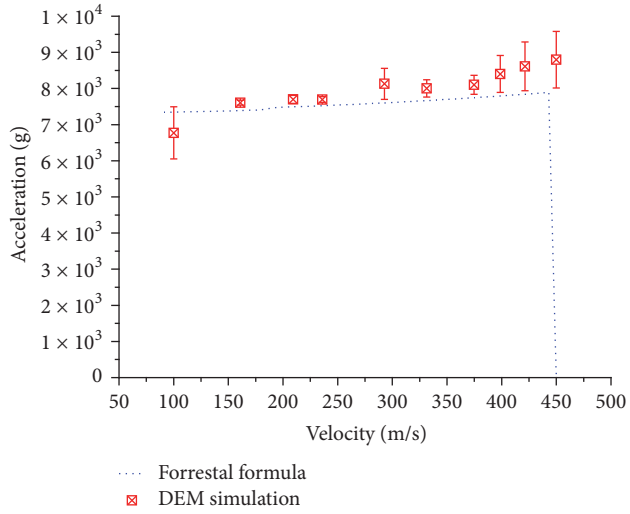

Figure 13: History of penetration acceleration as penetration velocity.

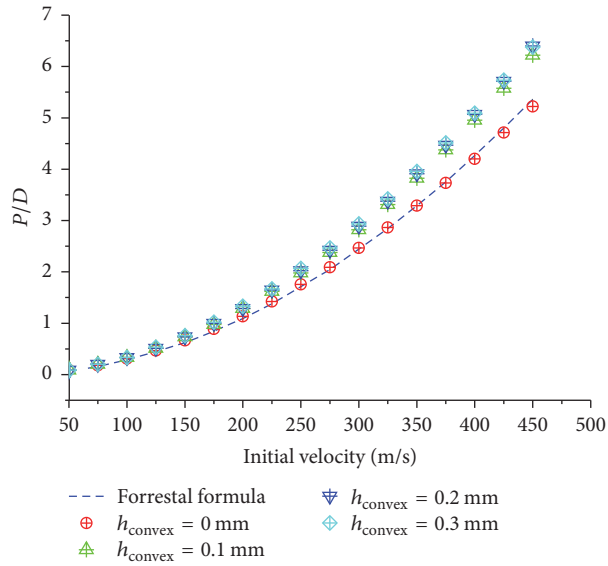

Figure 15: Ratio of penetration (P/D) with initial velocity.

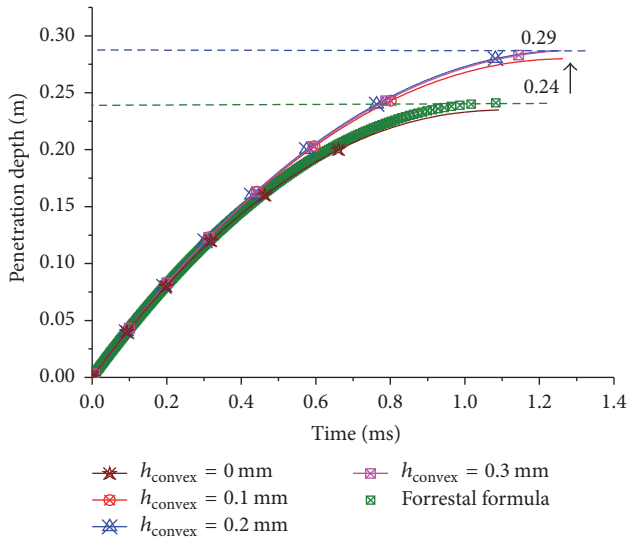

Figure 14: History of penetration depth with initial velocity of 450 m/s.

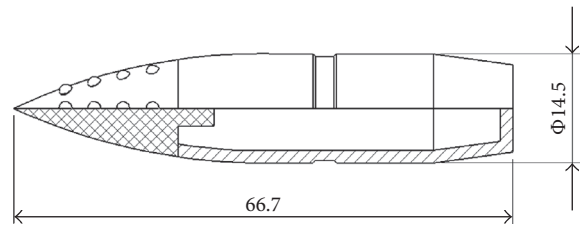

Figure 16: Structure of experiment projectile.

contact stiffness, and friction, especially the relative velocity between the contact particles. Therefore, the overload results of DEM simulation are more sensitive with the penetration velocity, which is also closer to the reality. Through the integration of acceleration, Figure 14 gives the history of the penetration depth. It shows that the maximum of final penetration depth obtained by h_{convex} = 0.3 mm increases from 0.24 m to 0.29 m under the same initial velocity of 450 m/s.

Figure 15 shows the relationship between the ratio of penetration (P/D is the ratio of penetration depth P with projectile diameter D) and initial velocity from 50 m/s to 450 m/s. It can be seen that the drag reduction for nonsmooth surface is very significant until the initial velocity reaches more than 200 m/s.

4.3. Experimental Verification. The comparative experiments were performed by the authors to validate the effect of the convex projectile nose surface on the penetrating performance. As for the projectile traditional alloy material it is not easy to process the convex array structure, so a kind of toughening ceramics for convex projectile nose shape by the method of 3D printing is selected. The strength and breaking tenacity of this kind material are 1200 Mpa and 15.0 Mpa, respectively. In order to guarantee the coaxiality, the nose structure was designed to be solid core with the bottom cylinder-shaped boss, which was mounted and cohered with the metal bullet core; the composite structure of projectile is shown in Figure 16.

Figure 17 shows the experimental projectiles with 14.5 mm diameter and 66.7 mm length, where the total weight of each one was about 59 g. The impact velocities of the projectiles were measured by a velocity sensors installed between the accelerating tube and the concrete target. The size of the concrete target is Φ1000 mm × 500 mm and its static compressive strength is 35 Mpa and the experiment

Table 2: The results of experiment and simulation.

Number	Mass (g)	Velocity (m/s)	Zone of crater (m)	Diameter of tunnel (m)	Penetration depth (m)		
					Experiment	Simulation	Forrestal formula
S-1	52.8	398	0.47 × 0.49	—	0.051	0.054	0.053
C-1	53.3	402	0.55 × 0.59	—	0.055	0.058	—
S-2	53.1	651	0.52 × 0.53	0.027	0.123	0.142	0.130
C-2	52.9	647	0.48 × 0.62	0.055	0.141	0.164	—

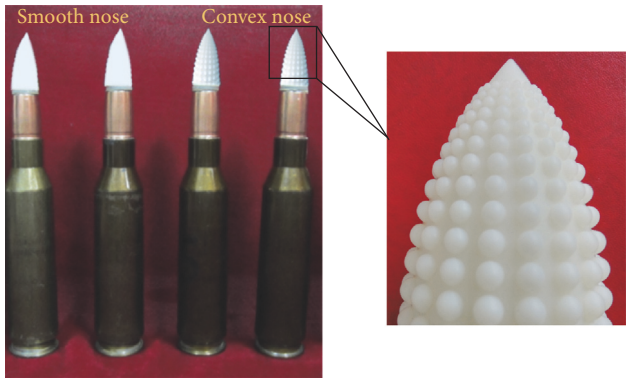

Figure 17: Experimental projectiles.

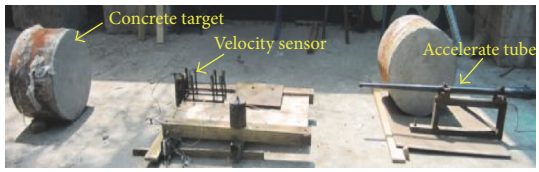

Figure 18: Experimental set-up for penetration.

set-up is shown in Figure 18. In this test, the impact velocities of the projectiles varied from about 400 m/s to 650 m/s.

As shown in Figure 19 and Table 2, when the projectiles impacted the test targets with initial velocities of about 400 m/s, only craters were formed on the front of the concrete targets. However, with the increase of impact velocity from 400 m/s to 650 m/s approximately, the concrete targets got more serious damage and the radial cracks, penetrating tunnel, and crater appeared simultaneously. In contrast with the traditional smooth nose surface S-1, the convex nose projectile with an initial velocity of 402 m/s C-1 would get a larger radial damage crater area of the concrete target. Similarly, the size of tunnel impacted by the convex nose projectile with the impact velocity 647 m/s C-2 was also larger than that of the smooth surface S-2 at the same condition. This experimental phenomenon reflects that the convex nose structure enlarges the radial contact zone and strengthens the radial flow of broken concrete fragments. Meanwhile, the ability of the penetration depth caused by the convex structure would be improved remarkably from 7.8% to 14.6% when the initial impact velocity changes from 400 m/s to 650 m/s. This trend is also proved by the results obtained from the above simulation. On the other hand, it is noted that the experimental results are consistent with the calculation by Forrestal's empirical formula for traditional smooth surface projectile and the numerical values by DEM simulation are slightly deviated as a whole, but the maximum relative error is less than 20%. This reason we concluded is that in our simulation the model is found in ideal conditions and some effect factors are ignored like angle of attack, mass abrasion, and so on, which is worth further study for us.

5. Conclusion

Inspired by the body surface of creature, especially the dung beetles, the effect of convex nonsmooth projectile nose surface on penetrating concrete target was investigated by the discrete element approach. In fact, relative to the dung beetle contacting with the soil, the penetrating problem of the projectile against concrete target has its uniqueness, like material property, damage pattern, and so on. Accordingly, the effects of convex structure on the antidrag and antifriction are also different. Thus, the mechanism of convex surface projectile with concrete target should be clarified firstly.

The DEM model for concrete target can be built where it is easier to capture the breakage and flow behavior of the projectile and concrete target interface in the penetration process. A PBM model was used to describe the adhesive property of concrete particle and the parameters were calibrated by a series of compression tests. This work shows that it is possible to simulate the process of concrete breakage and predict the resistance and distance of projectile in process of penetration.

The status of penetration shows that the convex improves the normal contact pressure of projectile-particle at certain velocity, which results in strengthening the concrete breakage and decreasing the radial constraint locating around the projectile tip. Meanwhile, the factors of more angular energy of broken particle and less contact area may contribute to decreasing the friction of projectile.

By fitting the limiting penetration resistance at a series of constant velocity the penetration acceleration and distance of projectile can be obtained. The experiments proved that the DEM method is suitable to predict the projectile performance and the antidrag effect of convex nose surface increases with the increasing of initial penetration velocity.

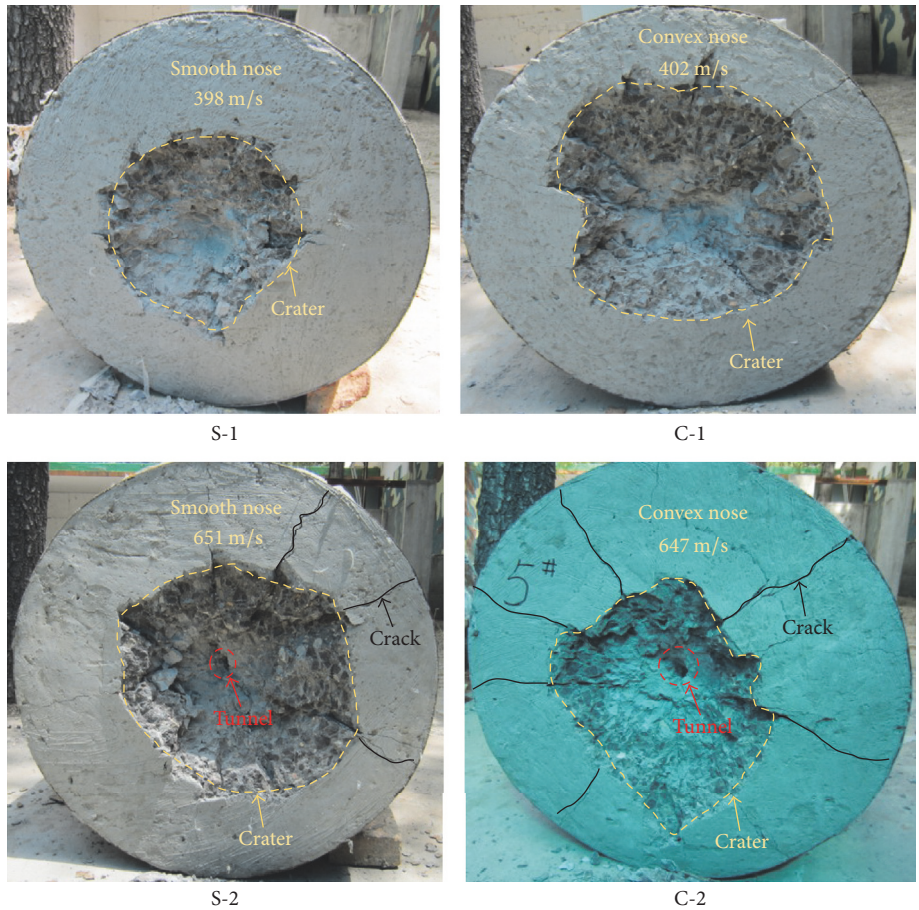

Figure 19: Damage of the concrete targets with different impact velocities.

Conflicts of Interest

The authors declare that there are no conflicts of interest regarding the publication of this paper.

Acknowledgments

This research is financially supported by the China Postdoctoral Science Foundation (2015M571289).

References

[1] X. W. Chen and Q. M. Li, "Deep penetration of a non-deformable projectile with different geometrical characteristics," *International Journal of Impact Engineering*, vol. 27, no. 6, pp. 619–637, 2002.

[2] G. Ben-Dor, A. Dubinsky, and T. Elperin, "Localized interaction models with non-constant friction for rigid penetrating impactors," *International Journal of Solids and Structures*, vol. 44, no. 7-8, pp. 2593–2607, 2007.

[3] L. Ren, J. Q. Li, and B. C. Chen, "Unsmoothed surface on reducing resistance by bionics," *Chinese Science Bulletin*, vol. 10, pp. 77–80, 1995.

[4] L. Ren, Z. Han, J. Li, and J. Tong, "Effects of non-smooth characteristics on bionic bulldozer blades in resistance reduction against soil," *Journal of Terramechanics*, vol. 39, no. 4, pp. 221–230, 2002.

[5] Z. Han, Z. Mu, W. Yin et al., "Biomimetic multifunctional surfaces inspired from animals," *Advances in Colloid and Interface Science*, vol. 234, pp. 27–50, 2016.

[6] Z. Wang, Z. Zhang, Y. Sun et al., "Wear behavior of bionic impregnated diamond bits," *Tribology International*, vol. 94, pp. 217–222, 2016.

[7] P. A. Cundall and O. D. L. Strack, "The distinct numerical model for granular assemblies," *Géotechnique*, vol. 29, no. 1, pp. 47–65, 1979.

[8] D. O. Potyondy and P. A. Cundall, "A bonded-particle model for rock," *International Journal of Rock Mechanics and Mining Sciences*, vol. 41, no. 8, pp. 1329–1364, 2004.

[9] W. Shiu, F. V. Donzé, and L. Daudeville, "Penetration prediction of missiles with different nose shapes by the discrete element numerical approach," *Computers & Structures*, vol. 86, no. 21-22, pp. 2079–2086, 2008.

[10] Y. Zhou, *Simulation of High-velocity penetration for rigid projectile into plain concrete target using discrete element method [M.S. thesis]*, Virginia Polytechnic Institute and State University, 2009.

[11] N. J. Brown, *Discrete Element modeling of cementitious materials [Ph.D. thesis]*, University of Edinburgh, 2013.

[12] J. Quist and C. M. Evertsson, "Cone crusher modelling and simulation using DEM," *Minerals Engineering*, vol. 85, pp. 92–105, 2016.

[13] J. Tong, M. A. Mohammad, J. Zhang et al., "DEM Numerical simulation of abrasive wear characteristics of a bioinspired ridged surface," *Journal of Bionic Engineering*, vol. 7, no. 2, pp. 175–181, 2010.

[14] E. R. Da Cunha, R. M. De Carvalho, and L. M. Tavares, "Simulation of solids flow and energy transfer in a vertical shaft impact crusher using DEM," *Minerals Engineering*, vol. 43-44, pp. 85–90, 2013.

[15] J. Tong, J. Sun, D. Chen, and S. Zhang, "Geometrical features and wettability of dung beetles and potential biomimetic engineering applications in tillage implements," *Soil & Tillage Research*, vol. 80, no. 1-2, pp. 1–12, 2005.

[16] A. Janda and J. Y. Ooi, "DEM modeling of cone penetration and unconfined compression in cohesive solids," *Powder Technology*, vol. 293, pp. 60–68, 2016.

[17] D. J. Frew, S. J. Hanchak, M. L. Green, and M. J. Forrestal, "Penetration of concrete targets with ogive-nose steel rods," *International Journal of Impact Engineering*, vol. 21, no. 6, pp. 489–497, 1998.

[18] M. J. Forrestal, D. J. Frew, J. P. Hickerson, and T. A. Rohwer, "Penetration of concrete targets with deceleration-time measurements," *International Journal of Impact Engineering*, vol. 28, no. 5, pp. 479–497, 2003.

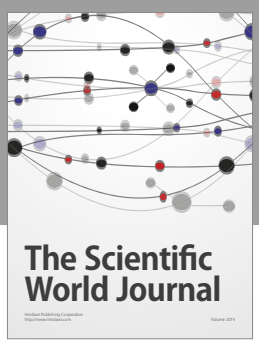

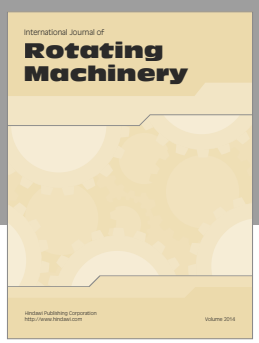

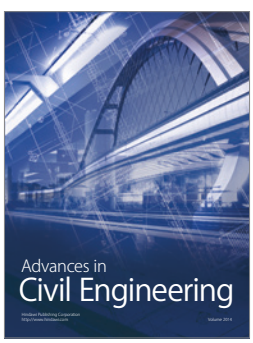

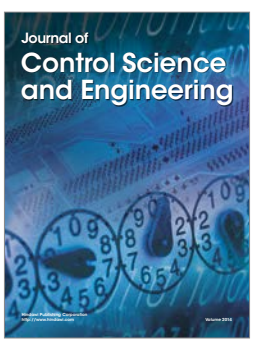

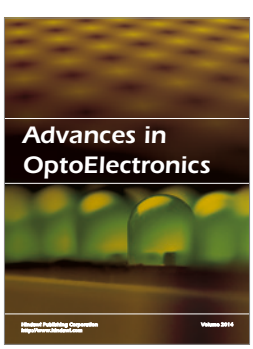

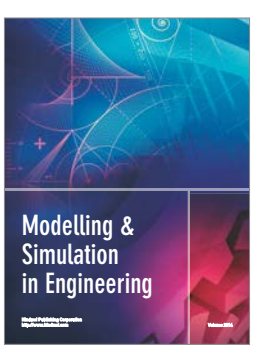

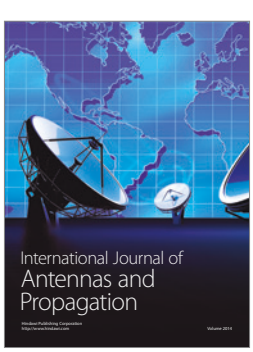

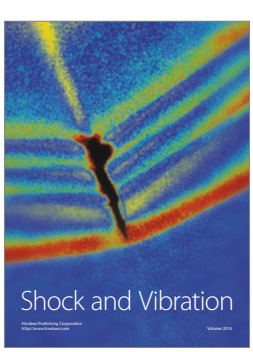

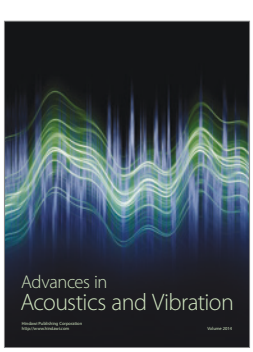

Hindawi

Submit your manuscripts at
https://www.hindawi.com